

# Preparation of Zn-doped TiO<sub>2</sub> nanoparticles decorated on graphene for photocatalytic degradation of tetracycline

FENG-JUN ZHANG<sup>a</sup>, RI-SHENG LI<sup>a</sup>, JIA-MING LI<sup>a</sup>, CHENG-JIA LIU<sup>a,b</sup>, CHAO JIANG<sup>a,b</sup>, CHUN-LI KANG<sup>a,\*</sup>

<sup>a</sup>Key Lab of Groundwater Resources and Environment, Ministry of Education, Jilin University, Changchun 130026, P. R. China

<sup>b</sup>China Power Engineering Consulting (Group) Corporation Northeast Electric Power Design Institute co., LTD. Changchun 130021, China

Zn-doped Titanium dioxide nanoparticles decorated on graphene sheets (ZT-GR) were synthesized via one step hydrothermal method. This method was to mix graphene oxide with Zn-doped Titanium dioxide in ethanol through a certain. The photocatalytic activity of this catalyst was assessed by photodegradation of tetracycline to verify. Graphene oxide amount and hydrothermal temperatures were discussed in this article. We discovered that the photocatalytic activity of Zn-doped TiO<sub>2</sub> nanoparticles decorated on graphene is much higher than Zn-doped TiO<sub>2</sub> nanoparticles through photocatalytic degradation experiments. Zn-doped TiO<sub>2</sub> on graphene sheets sample exhibited the highest photocatalytic activity when the graphene oxide amount was 5%, the hydrothermal temperature was 140 °C, the hydrothermal time was 24 hours. Graphene decorating not only narrowed the band gap also increased the optical absorption into visible region. The optimal degradation rate of TC by using the catalyst of Zn-doped TiO<sub>2</sub> nanoparticles decorated on graphene sheets was 98.5%. And graphene oxide decorating exhibited a good effect of degradation for tetracycline under visible light.

(Received August 1, 2016; accepted February 10, 2017)

**Keywords:** Zn-doped TiO<sub>2</sub>, Graphene, Sol-hydrothermal, Photocatalytic, Tetracycline degradation

## 1. Introduction

A long period of time in recently years, Titanium dioxide has caused a lot of concern in the control of environmental pollutants owing to its special properties, such as high chemical stability, easy to be obtained, low energy consumption, avirulence and high efficient recycling rate factor [1-4]. On the opposite side, Titanium dioxide still has some negative factors. For instance, it has problems in the recombination of photogenerated electron holes. Also, its range of visible light absorption is limited. The above reasons have induced photocatalysis of TiO<sub>2</sub> to have a low activity. Therefore, some researchers have made many new approaches to shift the optical absorption of TiO<sub>2</sub> to visible light region, and their final purpose is to improve the photocatalytic activity of TiO<sub>2</sub>. For instance, some researchers have extended the spectral response of TiO<sub>2</sub> into the visible light region by doping metals [5-8]. However, they created some as the photogenerated electrons and holes recombination center, it will be harmful to the photocatalytic process defect states. Another effective method to make the photocatalytic efficiency of TiO<sub>2</sub> higher is to immobilize TiO<sub>2</sub> with an absorbent surface such as zeolites, alumina, silica or carbon-based materials. In these materi-

als, carbonaceous materials, including activated carbon, carbon nanotubes and graphene, because of their unique porous structure are of great interest, electrical properties, adsorption capacity, and acidity [9-11]. And graphene research is also an important point of this article.

Graphene has a two-dimensional lattice plane of the film which composed of a single layer of carbon atoms, and it has a unique structure of honeycomb. Carbon atoms existed with sp<sup>2</sup> hybrid orbital arrangement, each carbon atom has four valence electrons. Carbon atoms were connected with very polar  $\sigma$  bond. There was left alone electron  $\pi$  after  $\sigma$  bond was formed  $\pi$  bond that moving freely in track can improve the conductivity and electron mobility of graphene. The characteristics of graphene has attracted a lot of concern due to its superior performance, electrical properties, optical properties and large specific surface area [12].

In addition, graphene has faster electron mobility to combine electronic with cavity. Graphite also has many advantages, such as its high surface area, completely transparent, and good interface with other adsorbents compared with Zn-doped TiO<sub>2</sub>. All in all, it has many advantages to investigate more simple and effective methods in the light of the catalytic reform. Besides, it is quite sig-

nificant to obtain the optimal photocatalytic function under visible light.

In this paper, Zn-doped TiO<sub>2</sub> nanoparticles were synthesized by sol-gel method. Zn-doped TiO<sub>2</sub> on graphene nanocomposites were obtained on the basis of the above method. At the same time, the effects of graphene amount and hydrothermal temperature were discussed. Furthermore, the photocatalytic activity of Zn-doped TiO<sub>2</sub> on graphene nanocomposites were evaluated by photocatalytic degradation of tetracycline. The structure characteristics characterization and analysis of as-prepared samples were studied by XRD, BET, XPS, UV-vis DRS, FT-IR and SEM.

## 2. Materials and methods

### 2.1. Materials

Tetrabutyl titanate (Ti(OC<sub>4</sub>H<sub>9</sub>)<sub>4</sub>) and Zinc chloride (ZnCl<sub>2</sub>) were obtained from Tianjin Guangfu Institute of Fine Chemicals (China). Absolute ethyl alcohol (CH<sub>3</sub>CH<sub>2</sub>OH) and Acetic acid (CH<sub>3</sub>COOH) were obtained from Beijing Chemical Works (China). Nitric acid (HNO<sub>3</sub>) was obtained from Xilong Chemical Co, LTD (China). Sulfuric acid (98%), K<sub>2</sub>S<sub>2</sub>O<sub>8</sub> and Sodium hydroxide (NaOH) was obtained from Beijing Chemical Works (China). Hydrochloric acid (HCl) was obtained from Beijing Chemical Works (China). All the reagents were of analytical grade and were used without further purification. The water used was distilled.

### 2.2. Synthesis of photocatalysts

#### 2.2.1. Synthesis of Zn-doped TiO<sub>2</sub>

Zn-doped TiO<sub>2</sub> was prepared via sol-gel method. The procedure was as follows: solution A was consisted of 8 mL CH<sub>3</sub>COOH, 24 mL CH<sub>3</sub>CH<sub>2</sub>OH, 6.4 mL of ZnCl<sub>2</sub> and 5 mL H<sub>2</sub>O. Then solution A was added drop by drop to the solution B. The solution B consists of 32 mL Ti(OC<sub>4</sub>H<sub>9</sub>)<sub>4</sub> and 80 mL CH<sub>3</sub>CH<sub>2</sub>OH. The obtained homogeneous solution was magnetically stirred for 1h and then aged at room temperature for 24h to form a gel. Then the gel was washed by water for several times and dried in an oven at 120 °C for 12h. The dry gel was calcined in a muffle furnace at 450 °C for 1h. The molar ratio of Zn in the sample was 5.0%. The as-prepared sample was denoted as ZT [13].

#### 2.2.2. Synthesis of GO

The improved Hummer's method used to configure graphene oxide. The procedure was as follows: solution A was consisted of 12ml concentrated H<sub>2</sub>SO<sub>4</sub>, 2.50 g of P<sub>2</sub>O<sub>5</sub> and 2.50 g of K<sub>2</sub>S<sub>2</sub>O<sub>8</sub>. Then 3.00 g of graphite powder was

added drop by drop to the solution A. The mixture was heated to 80 °C, mixed and stirred in a water bath for 5 hours. In 500ml of deionized water to dilute the suspension line. To obtain the desired solution by filtration, and washed with deionized for three times, dried at room temperature. The oxidized graphite was added to the 460 mL of H<sub>2</sub>SO<sub>4</sub> in an ice bath. Later, 60 g of KMnO<sub>4</sub> was slowly added by the temperature of 10 °C. Continue to stir at 35 °C for 2 h, then 920 ml of deionized water was added slowly by keeping the temperature below 50 °C. The 2.8 L of deionized water and 50 ml of 30% H<sub>2</sub>O<sub>2</sub> were slowly added to the mixture after 2 h. The mixture was centrifuged and washed by 5 L of 10% HCL solution, and then removed the acid by 5 L of deionized water. The obtaining solid was subjected to dialysis for a week. At last, the resulting product was dried in vacuo at room temperature [14]. After the detection of the solution, the solution of graphene oxide with a concentration of 16mg/ml.

#### 2.2.3. Synthesis of Zn-TiO<sub>2</sub> graphene nanocomposite

Zn-TiO<sub>2</sub>-graphene (ZT-GR) nanocomposites were synthesized by hydrothermal method. The procedure was as follows: The previous step configured solution of graphene oxide was diluted to 1mg/ml as the next backup solution. Deionized water (20 mL) and ethanol (10 mL) with different volume (2.0 mL, 4.0 mL, 10 mL, 20 mL, 30 mL, respectively) of GO by ultrasonic treatment for 1 h. Then 0.2 g of the ZT nanoparticles calcined at 450 °C was added to this solution and stirred for 3 h to get a homogeneous suspension. Then, the suspension was placed in a 100 mL Teflon-sealed autoclave and heated at different hydrothermal temperature (100 °C, 120 °C, 140 °C, 160 °C, 180 °C) for 24 h for reducing graphene oxide to graphene and depositing of ZT nanoparticles on carbon substrate. Finally, the resulting nanocomposites were recovered by filtration, washed with deionized water for three times and dried at 60°C for 24 h. The amount of GO in the samples were 1.0 %, 2.0 %, 5.0 %, 10 %, 20 % and 30%, respectively. The as-prepared samples were denoted as ZT-GR-n-t, where n and t represents the amount of GO and the hydrothermal temperature, respectively. For example, ZT-GR-5-140 represented the photocatalyst was heated at 140 °C and the GO amount was 5 %. The pure Zn-doped TiO<sub>2</sub> was denoted as ZT and used as a reference.

### 2.3. Characterization

The crystal structures were examined with a powder X-ray diffractometer (XRD) (BRUKER D8 ADVANCE, Cu K $\alpha$ ,  $\lambda=1.54056$  Å). The Brunauer-Emmett-Teller (BET) surface area and Barrett-Joyner-Halenda (BJH) pore size distribution measurements were carried out with ASAP 2020 Micromeritics USA. Scanning electron microscope (SEM) images were recorded with a model XL 30 ESEM FEG from Micro FEI Philips at room temperature. UV-visible reflectance spectra (UV/Vis DSC) for the samples were collected on a UV-visible spectrometer

(UV-2550 UV/vis Spectrometer, Shimadzu). Fourier transform infrared spectrophotometer (FT-IR, Perkin-Elmer System 2000) was used to determine the specific functional groups. X-ray photoelectron spectra (XPS) analysis was conducted through an X-ray photoelectron spectrometer (Thermo ESCALAB 250) with an Al K $\alpha$  (1486.7 eV) X-ray source.

#### 2.4. Photocatalytic activity of photocatalysts

Photocatalytic experiments nanocomposite materials were started in a quartz reactor (total volume of 100ml), coupled with a xenon lamp (500W, 8500 lux). And 0.1g photocatalyst was dispersed into 100ml of the reaction solution.

The initial concentration of TC was 40 mg/L. Before irradiation, the solution was magnetically stirred for 0.5 h in dark conditions to conduct the adsorption-desorption equilibration.

After dark adsorption, the lamp lights were turned on to initiate the photocatalytic reactions. Samples (ca. 5ml) were measured for UV-vis analysis at 20min time intervals and then centrifuged for 10min at the rate of 9000 rpm. The concentration of TC in each degraded sample was determined spectrophotometrically at 356nm. The residual rate of TC was calculated by the following Eq. 1:

$$\text{Residual rate} = C/C_0 \times 100\%$$

Where  $C_0$  is the initial concentration of TC and  $C$  is the concentration of TC after photocatalytic degradation.

### 3. Result and discussion

#### 3.1. XRD analysis

The crystalline phases of GO, TiO<sub>2</sub>, Zn-doped TiO<sub>2</sub> were examined by XRD patterns, which are shown in Fig. 1a. According to the results of the XRD characterizations, a reflection peak of GO appeared at  $2\theta=10.4^\circ$ , which corresponded to the earlier result and indicated that GO was synthesized by the improved Hummers method successfully [11]. It is clear to see that the diffraction peaks of TiO<sub>2</sub> located at  $25.3^\circ$ ,  $37.8^\circ$ ,  $48.0^\circ$ ,  $53.9^\circ$ ,  $55.1^\circ$ ,  $62.7^\circ$ ,  $68.8^\circ$ ,  $70.03^\circ$  and  $75.0^\circ$  can be respectively indexed to the (101), (004), (200), (105), (211), (204), (116), (220), and (215) crystal planes of anatase TiO<sub>2</sub> (JCPDS card 21-1272), in fully consistent with the previous study[15]. The XRD patterns of Zn-doped TiO<sub>2</sub> nanoparticles are similar to that of TiO<sub>2</sub>, which indicates that due to the low Zn content, the possible impurities like zinc oxide were not detected. In addition, the characteristic peak of  $10.4^\circ$  almost disappeared after hydrothermal treatment, indicating that most of the GO was restored to graphene. And the oxygen-containing functional group of GO was removed[16]. However, the graphene diffraction peak of  $2\theta=10.4^\circ$  was shielded by the strong anatase TiO<sub>2</sub> diffraction peak of  $2\theta=25.6^\circ$ . And the diffracted intensity was

weakened because of the less graphene imported, so there was no strong diffraction peaks of graphene detected [17].

Fig. 1b shows XRD patterns of samples with different GO amount at  $140^\circ\text{C}$  for 24 h. According to the data, it could be seen that with GO amount increasing, diffraction peaks of the samples were hardly changed. It indicated that crystal form of ZT-5-450 wasn't changed by the recombination of GO, the crystal form of samples was mainly composed by anatase TiO<sub>2</sub>. And conclusions could be drawn that the GO decorating inhibited the growth of crystallite size. It was noted that GO increased lattice distortion of samples, which was confirmed by data in Table 1. Generally, smaller crystallite was attributed to greater lattice distortion caused by larger amount, which would also enhance the concentration of lattice defects and thus precipitate carrier recombination [18]. This implied that with the increasing quality ratio of ZT/GR, average particle size of samples were decreasing owing to the increasing of distortion level [19].

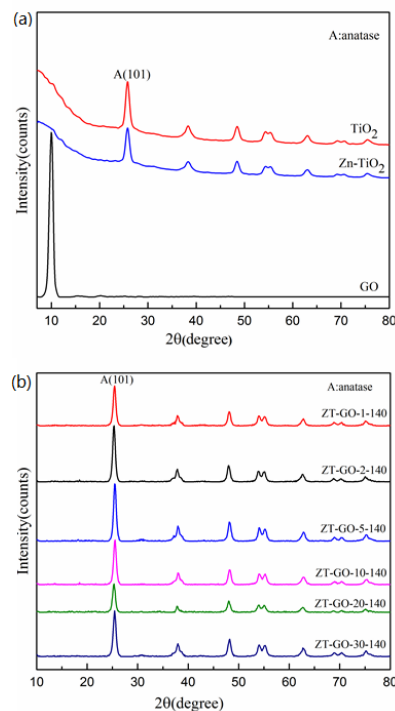


Fig. 1. XRD patterns of samples: a GO, TiO<sub>2</sub>, Zn-doped TiO<sub>2</sub>; b ZT-GR-n-140 with different GO amount

Table 1. Crystallite parameters of TiO<sub>2</sub> with different GO amount

Samples	Crystalline size/nm	lattice distortion
ZT-GO-1%-140	13.79	0.653
ZT-GO-2%-140	13.63	0.661
ZT-GO-5%-140	13.24	0.68
ZT-GO-10%-140	13.10	0.687
ZT-GO-20%-140	12.92	0.697
ZT-GO-30%-140	12.72	0.708

The crystallite sizes were calculated with the following Scherrer formula:

$$D = K\lambda / \beta \cos \theta$$

Where D parameter is the average crystallite size in angstroms, K parameter is a dimensionless constant (0.89 here),  $\lambda$  parameter is the wavelength of the X-ray radiation (Cu K $\alpha$ =0.15406 nm),  $\beta$  parameter is the full width at half-maximum (FWHM).

The resulting lattice distortions were calculated from the following Eq. 3:

$$\varepsilon = \beta / 4 \tan \theta$$

In which  $\varepsilon$  is lattice distortion and  $\theta$  is the diffraction angle [19]. Results were listed in Table 1.

### 3.2. BET analysis

The N<sub>2</sub> adsorption-desorption isotherm of ZT-5-450 and ZT-GR-5-140 indicated a specific surface area of 82.63 m<sup>2</sup>/g and 91.38 m<sup>2</sup>/g by BET analysis (Table 2) while the crystallite size of ZT-5-450 and ZT-GR-5-140 was 13.79 nm and 13.24 nm. It indicated that the samples with smaller crystallite size had larger surface area, which was in agreement with before studies.

Table 2. Surface area pore volume and pore size of ZT and ZT-GR

Sample	Surface area (m <sup>2</sup> /g)	Pore volume (cm <sup>3</sup> /g)	Pore size (BJH)(nm)
ZT-5-450	82.63	0.16	7.73
ZT-GR-5-140	91.38	0.18	7.61

Also, it indicated that compounding with graphene can increase the surface area of samples and the adsorption capacity of ZT-GR-5-140. The photocatalytic activity of ZT-GR was higher than ZT, which could be attributed to the large surface area of ZT-GR. The samples of pore size suggested that they were mesoporous nanoparticles. The stacking structure of graphene oxide sheets or the properties of graphene oxide maybe the reason that cause the porosity difference, and the factors above prevented the aggregation of Zn-doped TiO<sub>2</sub>. So, the surface area was increased. TC can be absorbed on the surface of graphene, thereby enabling TC to further degradation [20, 21].

### 3.3. SEM analysis

Fig. 2 shows the SEM images of TiO<sub>2</sub>, ZT, GO, ZT-GR. Fig. 2c shows that the lamellar structure of GO was glossy. And the sample of ZT-5-450 was consisted of

tightness and homogeneous anatase particles. It was obviously seen that wrinkle lamellar structure outline of graphene and particles of ZT-5-450 were dispersed on lamellar surface [22]. GO contained a large number of oxygen-containing functional groups such as hydroxy, carboxyl and titanium particles which combined with these active sites by the way of hydrogen bonding or electrostatic adsorption. ZT-5-450 nanoparticles still not separated with graphene which indicated that the hydroxyl of ZT-5-450 surface and the oxygen-containing functional groups of graphene sheet have had an interaction.

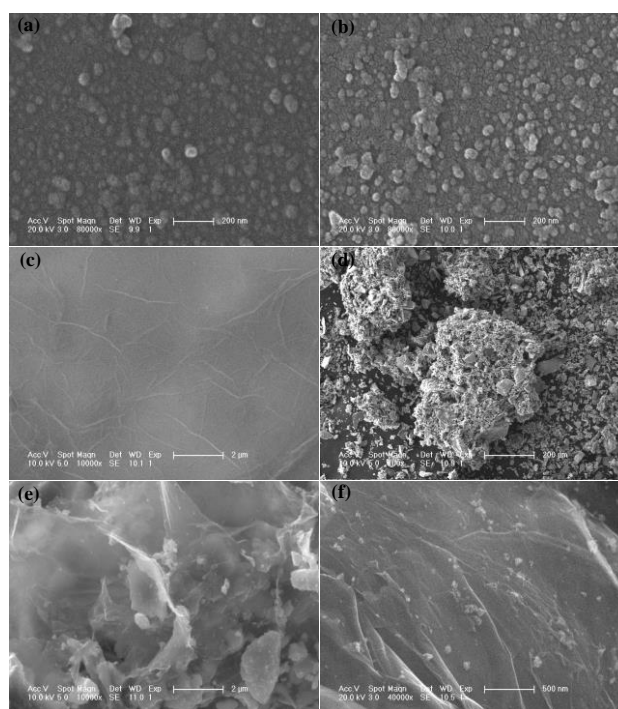


Fig. 2. SEM images of (a) TiO<sub>2</sub>, (b) Zn-doped TiO<sub>2</sub> nanoparticles, (c) GO, (d), (e), (f) ZT-GR-5-140.

The SEM images of Fig. 2d, e, f show that Zn-doped TiO<sub>2</sub> and graphene were well combined, also the Zn-TiO<sub>2</sub> nanoparticles were distributed well on the surface of carbon source [23]. As shown in Fig. 3, the EDX spectrum illustrated the presence of Zn component in the composite.

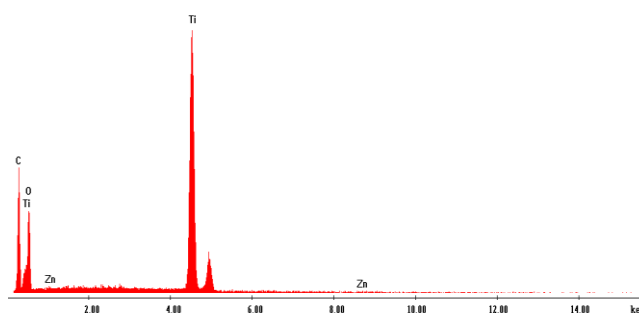


Fig. 3. EDX pattern of ZT-GR composite

### 3.4. FT-IR spectra

Fig. 4 shows the FT-IR spectra of the as-prepared GO, TiO<sub>2</sub>, Zn-TiO<sub>2</sub>, and Zn-TiO<sub>2</sub>-GR composite samples. In FT-IR spectrum of GO, the broad peak at 3420 cm<sup>-1</sup> is attributed to the hydroxyl stretching vibrations of the C-OH groups, and the peak at 1730 cm<sup>-1</sup> is assigned to the C=O stretching vibrations on the GO surface. Also, the peak at 1060 cm<sup>-1</sup> band is due to the C-O stretching vibrations [24]. These surfaces oxygen-containing functional groups render the possibility of covalent linkage of Zn-TiO<sub>2</sub> onto the GO surface. FT-IR spectra of Zn-TiO<sub>2</sub> and Zn-TiO<sub>2</sub>-GR composite show a strong absorption band around 500-1000 cm<sup>-1</sup> after TiO<sub>2</sub> deposition, which also shows the deposition of TiO<sub>2</sub> during the hydrothermal process. It is noteworthy that the C=O peak at 1730 cm<sup>-1</sup> disappears in the Zn-TiO<sub>2</sub>-GR sample, which is because of the reduction of GO to graphene during the hydrothermal process.

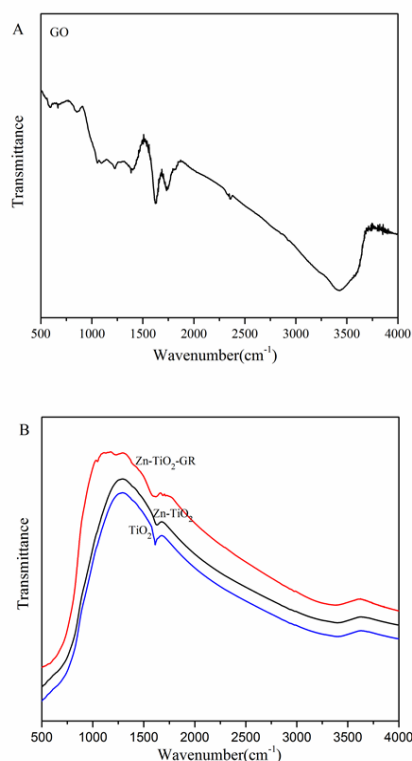


Fig. 4. FT-IR spectra of (A) graphene oxide, (B) TiO<sub>2</sub>, Zn-doped TiO<sub>2</sub> and Zn-TiO<sub>2</sub>-GR composite

### 3.5. UV-vis DRS analysis

The UV-visible absorption spectra of the Zn-doped TiO<sub>2</sub> nanoparticles with different GO amount are shown in Fig. 5. The UV-vis absorption spectrum of GO shows a peak at about 235 nm which is due to  $\pi \rightarrow \pi^*$  transitions of aromatic C=C bonds, and a shoulder at about 290-300 nm, corresponding to  $n \rightarrow \pi^*$  transition of the C=O bond [25]. After hydrothermal reduction treatment at 140 °C for 24h the absorption peak of GO at 235 nm red-shifts to higher

wavelength and the shoulder disappeared. In addition, Zn-doped TiO<sub>2</sub> displayed an absorption edge at about 400nm and graphene oxide showed a small absorbance peak at 235 nm. However, the red shifts into the longer wavelength regions occurred along with the stronger absorption intensity on Zn-TiO<sub>2</sub>-GR nanocomposites. Typically, the light absorption extended to 430, 460 and 470nm as incorporating graphene oxide into Zn-doped TiO<sub>2</sub> matrix with 1, 2 and 5wt%, respectively. But the light absorption decreased to 460nm as incorporating graphene oxide into Zn-doped TiO<sub>2</sub> matrix with 20 and 30wt%. The results obviously demonstrate the significant influence of graphene oxide on the optical characteristics in which increasing graphene oxide amount narrows the band gap of Zn-doped TiO<sub>2</sub>. Similar to the case of TiO<sub>2</sub>-CNT, C-doped TiO<sub>2</sub> or TiO<sub>2</sub>-chemically converted graphene composites, the phenomena in this study could be ascribed to the formation of Ti-O-C chemical bonding in the prepared composites [11, 26, 27].

The band gap was calculated by  $E_g = 1240/\lambda$ , where  $E_g$  (eV) is the band gap and  $\lambda$  (nm) is the wavelength of the absorption edge in the spectrum [28]. The results are shown in Table 3. The band gap energies decreased with GO amount increasing, suggesting that GO could be incorporated at a level near the valance band of TiO<sub>2</sub> thus reducing band gap [29].

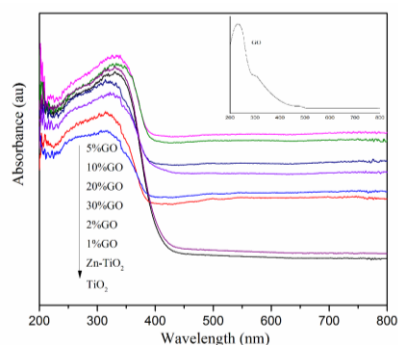


Fig. 5. UV-visible absorption of samples with different GO amount

Table 3. The band gap energies of samples with different GO amount

Sample	$\lambda$ (nm)	$E_g$ (eV)
ZT	416.91	2.97
ZTG-1%	432.15	2.87
ZTG-2%	445.44	2.78
ZTG-5%	472.51	2.62
ZTG-10%	470.21	2.63
ZTG-20%	460.88	2.69
ZTG-30%	459.43	2.51

### 3.6. XPS analysis

Fig. 6 shows the XPS spectra of Zn-doped TiO<sub>2</sub> on graphene composite. The composite contains 56.22% O1s, 16.18% Ti2p, 27.08% C1s and 0.52% Zn2p. In the level XPS spectrum of Ti2p core, the Ti2p<sub>3/2</sub> and 2p<sub>1/2</sub> for Zn-doped TiO<sub>2</sub> on graphene surface are located at binding energies 458.4 eV and 464.2 eV, respectively, which is consistent with the value of Ti<sup>4+</sup> in the TiO<sub>2</sub> lattice [30]. It is obviously seen that there exist two peaks at 529.8 eV and 531.7 eV in O1s core level spectrum, which are assigned to the metallic oxides (Ti-O) and the residual oxygen-containing groups in reduced graphene oxides [31], in agreement with the result of FT-IR (Fig. 4). In C1s core level XPS spectrum, the main peak was observed at 284.8 eV, which corresponds to the adventitious carbon adsorbed on the surface of sample [24]. The peak at 286.2 eV suggests the existence of C-O bond of carbonous species [32]. The peak at 289.25 eV corresponds to C=O bonds also shifted to lower binding energy (288.8 eV), clearly showing coordination bonding between Ti and carboxyl acids on graphene sheets [33].

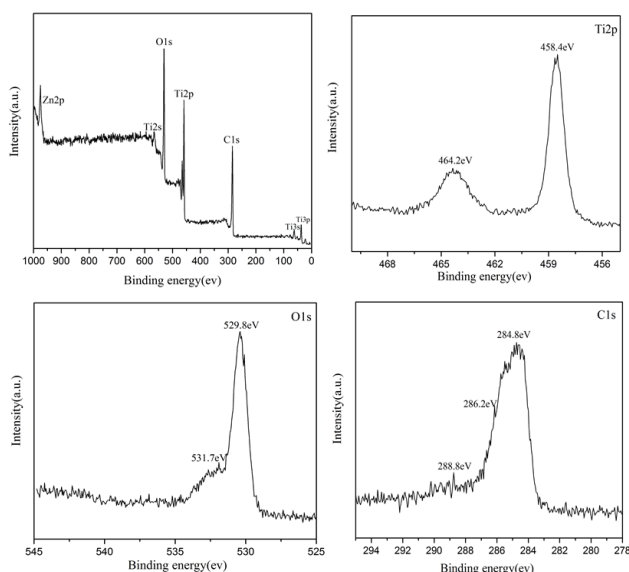


Fig. 6. XPS survey and core level spectra of Ti2p, O1s and C1s is region of ZT-GR sample

### 3.7. Photocatalytic activity

Fig. 7 shows the degradation rate of TC different GO amount. The degradation rate of TC for ZT within 120 min was 90%. The best conditions of ZT-GR had higher photocatalytic activity than did ZT. With increasing GO amount from 1% to 20%, the photocatalytic activity increased at first and the decreased at last, indicating that there was an optimal amount. The highest degradation rate of ZT-GR-5-140 reached 98.5% within 120min. The photocatalytic activity of ZT-GR-20-140 decreased to 82%. For high concentration of the GO amount, a portion of the transition metal ions would become the combination cen-

ter for the electrons and holes [34].

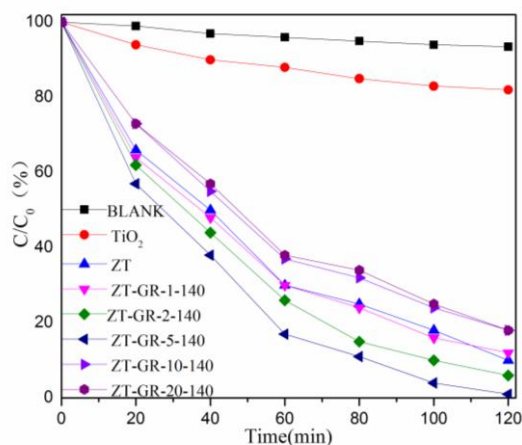


Fig. 7. Photocatalytic degradation of samples with different GO amount

Fig. 8 shows the effect of hydrothermal temperature on photocatalytic activity of samples. It could be seen that with hydrothermal time increasing, the photocatalytic degradation increased at first and the decreased at last. With further increasing hydrothermal temperature to 140 °C, the degradation rate was increasing to 98.5%. Then, when the hydrothermal temperature got to 180 °C, the degradation rate was decreased to 74%.

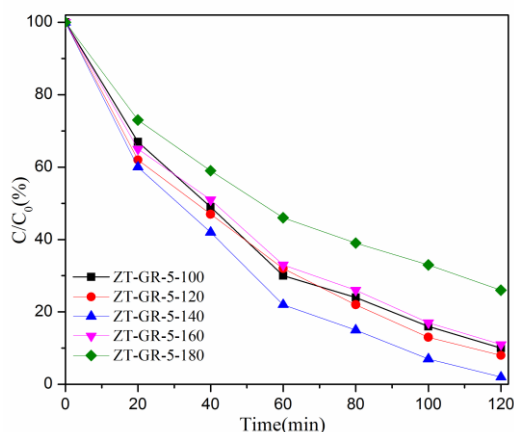


Fig. 8. Photocatalytic degradation of samples with different hydrothermal temperature

In addition, as a representative photocatalyst, an examination to the recycled photocatalytic activity of ZT-GR was also carried out, and the corresponding result was presented in Fig. 9. In the four cyclic TC tests, the ZT-GR exhibited an excellent stability with an average TC removal efficiency, and no evident change has taken place for the photocatalytic activity, which indicates good photocatalytic stability of the ZT-GR catalyst.

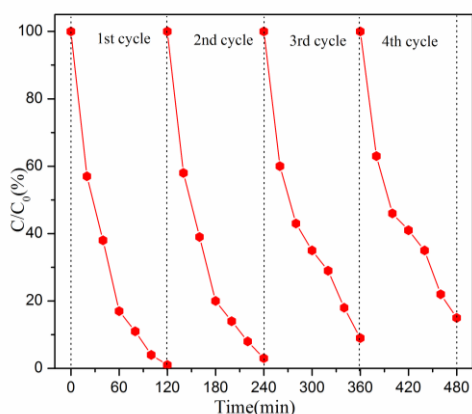


Fig. 9. Results of recycling experiment showing the initial run and a series of three recycling runs of ZT-GR-5-140

### 3.8. Proposed mechanism

Based on above results, a mechanism for the increased photocatalytic activity over the as-prepared ZT-GR catalyst is proposed as follows:



When the ZT-GR was irradiated with visible light in the presence of an aqueous solution of an organic compound (e.g., TC), Zn-doped  $\text{TiO}_2$  is excited by photons, and electron-hole pairs are generated (Eq. (1)). The photogenerated electrons can transfer readily from the conduction band (CB) of Zn-doped  $\text{TiO}_2$  to the surface of the graphene oxide (Eq. (2)). At the same time, electrons can be scavenged by  $\text{O}_2$  in the water, resulting in superoxide anion free radicals ( $\bullet\text{O}_2^-$ ) (Eq. (3)), which are the main active species in the reaction with TC. Moreover, the reactive holes at the valence band (VB) of Zn-doped  $\text{TiO}_2$  will oxidize TC directly.

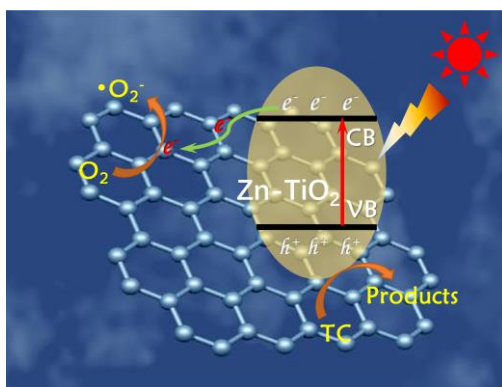


Fig. 10. Schematic photocatalytic mechanism for the ZT-GR catalyst under visible light irradiation

## 4. Conclusions

In this article, ZT-GR of different conditions were successfully synthesized by sol-hydrothermal without ready-made  $\text{TiO}_2$  powder. It was significantly proved that decorating graphene with ZT could enhance the activity of photocatalysis. Also, it was no obvious spacing change which was observed after GO decorating. The UV-visible absorption spectra of ZT-GR shifted remarkably to the visible region and the absorption enhanced significantly.

The as-prepared ZT-GR were demonstrated to have a higher photocatalytic activity for the degradation of TC under irradiation of visible light. It was found that ZT-GR exhibited the highest photocatalytic activity under visible light compared to ZT. The enhancement in the photocatalytic activity could be ascribed to the narrowing of band gap and the promoted separation of photogenerated electrons and holes. Moreover, the photocatalytic activity did not linearly increase with GO amount further increasing. All in all, in all experiments, ZT-GR with high photocatalytic activity were prepared by a convenient and effective sol-hydrothermal method, which could be engineered into the pollutants photodegradation of water under visible light.

## Acknowledgements

This work was supported by the Jilin Province Development and Reform Commission (No.2015y049), Jilin Province Science and Technology Development Project (No.20130101091JC), the analysis and testing foundation of Jilin University, Changchun Technology Innovation Fund (No. 2009086), Graduate Innovation Fund of Jilin University (Grant No.2016099) and National Natural Science Foundation of China (Grant No.41472214).

## References

- [1] N. Khalid, E. Ahmed, Z. Hong, Y. Zhang, M. Ahmad, *Current Applied Physics* **12**, 1485 (2012).
- [2] J.-G. Huang, S. Pang, B. Wang, et al., *Optoelectron. Adv. Mat.* **9**(1-2), 139 (2015).
- [3] J.-G. Huang, X.-T. Guo, B. Wang, et al., *Journal of Spectroscopy* **2015**, 1 (2015).
- [4] X. Li, R. Xiong, G. Wei, *Journal of Hazardous Materials* **164**, 587 (2009).
- [5] T. Umebayashi, T. Yamaki, H. Itoh, K. Asai, *Journal of Physics and Chemistry of Solids* **63**, 1909 (2002).
- [6] D. Dvoranova, V. Brezova, M. Mazúr, M. A. Malati, *Applied Catalysis B: Environmental* **37**, 91 (2002).
- [7] Z. Ambrus, N. Balázs, T. Alapi, et al., *Applied Catalysis B: Environmental* **81**, 27 (2008).
- [8] M. Anpo, M. Takeuchi, *Journal of Catalysis* **216**, 505 (2003).
- [9] J. Matos, A. Garcia, T. Cordero, J.-M. Chovelon, C.

- Ferronato, *Catalysis Letters* **130**, 568 (2009).
- [10] K. Woan, G. Pyrgiotakis, W. Sigmund, *Adv. Mater* **21**, 2233 (2009).
- [11] H. Zhang, X. Lv, Y. Li, Y. Wang, J. Li, *ACS Nano* **4**, 380 (2009).
- [12] S. Wang, S. Zhou, *Journal of Hazardous Materials* **185**, 77 (2011).
- [13] A. Peigney, C. Laurent, E. Flahaut, R. Bacsu, A. Rousset, *Carbon* **39**, 507 (2001).
- [14] Y. Li, Y. Wu, *Journal of the American Chemical Society* **131**, 5851 (2009).
- [15] J. Liu, H. Bai, Y. Wang, Z. Liu, X. Zhang, D. D. Sun, *Advanced Functional Materials* **20**, 4175 (2010).
- [16] N. Khalid, Z. Hong, E. Ahmed, Y. Zhang, H. Chan, M. Ahmad, *Applied Surface Science* **258**, 5827 (2012).
- [17] C. Nethravathi, M. Rajamathi, *Carbon* **46**, 1994 (2008).
- [18] C. Burda, Y. Lou, X. Chen, A. C. Samia, J. Stout, J. L. Gole, *Nano Letters* **3**, 1049 (2003).
- [19] S.-Y. Luo, B.-X. Yan, J. Shen, *Thin Solid Films* **522**, 361 (2012).
- [20] D. S. Bhatkhande, V. G. Pangarkar, A. A. Beenackers, *Journal of Chemical Technology and Biotechnology* **77**, 102 (2002).
- [21] W. Low, V. Boonamnuayvitaya, *Journal of Environmental Management* **127**, 142 (2013).
- [22] G. Li, T. Wang, Y. Zhu, et al., *Applied Surface Science* **257**, 6568 (2011).
- [23] C. Li, D. Zhang, Z. Jiang, Z. Yao, F. Jia, *New Journal of Chemistry* **35**, 423 (2011).
- [24] S. Ghasemi, S. R. Setayesh, A. Habibi-Yangjeh, M. Hormozi-Nezhad, M. Gholami, *Journal of Hazardous Materials* **199**, 170 (2012).
- [25] S. Y. Treschev, P.-W. Chou, Y.-H. Tseng, J.-B. Wang, E. V. Perevedentseva, C.-L. Cheng, *Applied Catalysis B: Environmental* **79**, 8 (2008).
- [26] Y. Zhou, Q. Bao, L. A. L. Tang, Y. Zhong, K. P. Loh, *Chemistry of Materials* **21**, 2950 (2009).
- [27] X.-Y. Zhang, H.-P. Li, X.-L. Cui, Y. Lin, *J. Mater. Chem.* **20**, 2801 (2010).
- [28] Y. Yao, G. Li, S. Ciston, R. M. Lueptow, K. A. Gray, *Environmental Science & Technology* **42**, 4952 (2008).
- [29] Y.-J. Xu, Y. Zhuang, X. Fu, *The Journal of Physical Chemistry C* **114**, 2669 (2010).
- [30] J.-G. Huang, M.-Y. Zheng, S. Pang, et al., *Reaction Kinetics, Mechanisms and Catalysis* **113**, 281 (2014).
- [31] J. C. Yu, J. Yu, W. Ho, Z. Jiang, L. Zhang, *Chemistry of Materials* **14**, 3808 (2002).
- [32] B. Erdem, R. A. Hunsicker, G. W. Simmons, E. D. Sudol, V. L. Dimonie, M. S. El-Aasser, *Langmuir* **17**, 2664 (2001).
- [33] Y. Wu, J. Zhang, L. Xiao, F. Chen, *Applied Surface Science* **256**, 4260 (2010).
- [34] T. Ohno, T. Tsubota, M. Toyofuku, R. Inaba, *Catalysis Letters* **98**, 255 (2004).

---

\*Corresponding author: kangchunli2002@163.com